Ultrasonics Sonochemistry 80 (2021) 105830

Contents lists available at ScienceDirect

Ultrasonics Sonochemistry

journal homepage: www.elsevier.com/locate/ultson

Fabrication and characterization of quercetin loaded casein phosphopeptides-chitosan composite nanoparticles by ultrasound treatment: Factor optimization, formation mechanism, physicochemical stability and antioxidant activity

Qiufang Liang [a,b], Xinru Sun [a], Husnain Raza [a], Muhammad Aslam Khan [d], Haile Ma [a,b,c], Xiaofeng Ren [a,b,c,*]

[a] School of Food and Biological Engineering, Jiangsu University, 301 Xuefu Road, Zhenjiang, Jiangsu 212013, China
[b] Jiangsu Provincial Key Laboratory for Physical Processing of Agricultural Products, Zhenjiang, Jiangsu 212013, China
[c] Institute of Food Physical Processing, Jiangsu University, 301 Xuefu Road, Zhenjiang, Jiangsu 212013, China
[d] State Key Laboratory of Food Science and Technology, Jiangnan University, Wuxi, Jiangsu 214122, China

ARTICLE INFO

Keywords:
Ultrasound
Encapsulation
Casein phosphopeptides
Chitosan
Stability
Antioxidant activity

ABSTRACT

Ultrasound treatment was used to successfully prepare Quercetin (Qu)-loaded Casein phosphopeptides (CPP)/chitosan (CS) nanoparticles. Compared with the control, the above ternary nanoparticles with the smallest size (241.27 nm, decreased by 34.32%), improved encapsulation efficiency of Qu (78.55%, increased by 22.12%) when prepared under following conditions: ultrasonic frequency, 20/35/50 kHz; the power density, 80 W/L; the time, 20 min, and the intermittent ratio, 20 s/5s. Electrostatic interactions, hydrogen bonding, and hydrophobic interactions were the main driving forces for nanoparticles formulation, which were strengthened by ultrasound treatment. The compact, homogeneous and spherical composite nanoparticles obtained by sonication were clearly observed by scanning electron microscope and atomic force microscope. The environmental stability (NaCl, pH, exposure time, storage time, and simulated gastrointestinal digestion) and antioxidant activity of the ternary nanoparticles were remarkably enhanced after ultrasonic treatment. Furthermore, the ternary nanoparticles prepared by ultrasound exhibited excellent stability in simulated gastrointestinal digestion. The above results indicate that ultrasound not only increases the loading of the nanoparticles on bioactive substances but also improves the environmental stability and antioxidant activity of the formed nanoparticles. Ultrasound-assisted preparation of nanoparticles loaded with bioactive substances could be well used in the functional food and beverage industry.

1. Introduction

Quercetin (Qu) (3,5,7,3,4-pentahydroxy flavone) is a natural flavanol found in diverse seeds, fruits, and vegetables including apple, onion, legumes, and chili peppers [1]. Recently, Qu has gained considerable attention owing to its multiple physiological benefits, such as antioxidant, anti-diabetic, and anti-inflammatory activity [2]; it is now considered as one of the best candidates as a nutritional supplement. However, the application of Qu is limited in food and clinical industries because of its inherent physicochemical instability, high hydrophobicity, and poor oral bioavailability [3]. The use of nanoparticle delivery systems to encapsulate Qu is an effective method to overcome these shortcomings. Because of their biocompatibility, non-toxicity, high nutritional value, and intrinsic biodegradability, natural compounds having nano-architectures, such as starch, lipids, polysaccharides, and proteins, are regarded as promising and effective delivery carriers [4].

The utilization of proteins and peptides to fabricate new nanoparticles for the delivery of bioactive compounds by molecular self-assembly has been the subject of extensive research for decades [5,6]. Protein-derived peptides have the same amphiphilic properties as proteins, and their smaller molecular weight and exposure to a large number of active groups lead to more advantages than proteins as embedding materials [7]. Furthermore, peptides can self-assemble in an orderly manner ("bottom-up" method and "top-down" strategy) to form

* Corresponding author at: School of Food and Biological Engineering, Jiangsu University, 301 Xuefu Road, Zhenjiang 212013, China.
E-mail address: renxiaofeng@ujs.edu.cn (X. Ren).

https://doi.org/10.1016/j.ultsonch.2021.105830
Received 22 October 2021; Received in revised form 5 November 2021; Accepted 12 November 2021
Available online 14 November 2021

regular nanostructures [8]. Zhang, Zhao, Ning, Yu, Tang and Zhou [9] found that self-assembled soy peptides could effectively control the release of curcumin at the intestinal stage and significantly improve its bioavailability. Wang, Yang, Patanavanich, Xu and Chau [10] reported a novel nanoparticle prepared by self-assembly of modified aromatic dipeptides triggered by enzymes that could be used for drug delivery. More relevant studies on peptide-related building blocks (including secondary amphiphilic peptides, cyclic peptides, surfactant-like oligopeptides, etc.) clearly showed that peptide-based nanostructures have a great potential as delivery vehicles for bioactive compounds [9]. Casein phosphopeptides (CPP), a phosphorylated bioactive peptide derived from casein, is widely used as a carrier for calcium delivery. Recent studies have found that the phosphate group (PO_4^{3-}) carried by CPP leads to its negatively charged groups of polyanion, which can be well combined with the cationic chitosan oligosaccharides [11]. Zhu, Hou and He [12] reported the chitosan (CS)/TPP shell structure formed via ionic gelation interactions showed appropriate colloidal stability, calcium-loading capacity and ability to delay digestion in gastrointestinal conditions. Taking into account the self-assembly properties of the peptide itself and the advantage that CPP can effectively form complexes with cationic polysaccharides, it is feasible to make a CPP/CS composite structure for encapsulation and delivery of bioactive compounds.

Owing to its special cavitation, heating, dynamic stirring, shear stress, and turbulence properties, ultrasound is increasingly applied in various research areas, including assisted enzymatic hydrolysis, assisted freezing, and extraction of bioactive components [13]. Recently, ultrasound technology has also been proven to be a very effective tool for improving the encapsulation efficiency of bioactive compounds. Liang, Ren, Zhang, Hou, Chalamaiah, Ma and Xu [14] reported that ultrasound treatment increased the encapsulation efficiency and loading capacity of resveratrol with zein as a carrier. The resveratrol-loaded zein-chitosan nanoparticles were successfully prepared by employing various ultrasound frequencies; and ultrasound treatment not only reduced the nanoparticle size but also narrowed their size distribution [15]. Essentially, the encapsulated effect of the bioactive compound is highly dependent on the protein/polysaccharide complexation structure, which is constructed through intermolecular interaction, including electrostatic repulsion, hydrogen bonding, surface hydrophilicity [16]. The ultrasound-induced unfolding of protein/polysaccharide-based macromolecules exposes their functional groups, which are otherwise buried in the native structure; unfolded macromolecules are more susceptible to intermolecular interaction [17,18]. The increased collision frequency between macromolecules induced by ultrasound is particularly important, as it improves their intermolecular interaction [19]. From another perspective, the alteration of intermolecular forces caused by ultrasound can also lead the resulting nanoparticles to undergo structural and functional changes, which indirectly determine the biological activity and environmental stability of the embedded compounds. However, just a few research on the bioactivity and environmental stability of nanoparticles produced by ultrasonic treatment have been reported.

Thus, the objectives of this study are: (a) to focus on the fabrication of CPP/CS complex with the excellent encapsulated capacity of Qu by ultrasound, (b) to characterize the structural properties of the Qu loaded CPP/ nanoparticles, (c) to evaluate the stability of ternary nanoparticles to environmental factors, including NaCl, pH, exposure time, storage time and simulate gastrointestinal digestion, (d) to analyze the antioxidant activity (DPPH radical scavenging rate, ABTS scavenging rate and Fe^{3+} reducing power) *in vitro* of the ternary nanoparticles prepared by ultrasound treatment.

2. Materials and methods

2.1. Materials

Casein phosphopeptides (CPP) (purity $\geq$ 80%) were purchased from Shanghai Yien Chemical Technology Co., Ltd. (Shanghai, China). CS (Deacetylation Degree 80.0–95.0%), Qu (purity $\geq$ 99%) were purchased from Sinopharm Group Chemical Reagent Co., Ltd. (Shanghai, China). Pepsin, Pancreatin and 2,2-diphenyl-1-picrylhydrazyl (DPPH) were bought from Sigma-Aldrich (St. Louis, MO, USA). Other reagents are of analytical grade.

2.2. Fabrication of Qu-loaded CPP/CS (CPP-CS-Qu) nanoparticles

In order to prevent Qu from being decomposed, all the treatments and determinations of Qu in the following paragraphs were carried out in the dark. Stock solutions of Qu, CPP and CS at a concentration of 1.5 mg/mL were prepared by dissolving them in absolute ethanol, distilled water and 1.0% (w/v) acetic acid, respectively. First, the Qu solution was mixed with CPP solution at a ratio of 1:5 (v/v) and stirred for 15 min. By consequential addition of the same volume of CS solution as CPP to the above suspension with further stirring for 15 min at room temperature, and the pH of the mixture was adjusted to 6 to form Qu-loaded CPP/CS nanoparticles. An equal volume of blank solution was used instead of Qu, CS solution to prepare CPP/CS (CPP-CS) complex, Qu-loaded CPP (CPP-Qu) nanoparticles, and other processing steps remained unchanged.

2.3. Ultrasound treatment of the CPP-CS-Qu nanoparticles

A multi-frequency power ultrasound equipment developed by our research team and manufactured by Meibo Biotechnology Co., Ltd (Zhenjiang, Jiangsu, China) was used to process the sample in this study (Liang et al., 2018). The CPP-CS-Qu nanoparticles prepared in section 2.2 were ultrasonicated immediately at various levels of ultrasound conditions as follows: different ultrasound frequency (single frequency, 20, 35, and 50 kHz; simultaneous dual-frequency 20/35, 20/50, and 35/50 kHz, and synchronous triple-frequency 20/35/50 kHz); different ultrasound time (5, 10, 15, 20 and 30 min); different ultrasound power density (30, 40, 60, 80 and 100 W/L); different ultrasound intermittent ratio (10 s/5s, 20 s/5s, 30 s/5s, 50 s/5s and continue working). When one of the above ultrasound conditions altered, the other ultrasound conditions were fixed as simultaneous dual-frequency 35/50 kHz, ultrasound power density 60 W/L, ultrasound time 10 min and ultrasound intermittent ratio 30 s/5s. During the entire ultrasonic treatment process, the temperature of the sample was controlled at 25 ℃ through a circulating water bath. The control sample was prepared using a magnetic stirrer instead of ultrasound and other conditions remained unchanged.

According to the results of the above ultrasound single-factor tests, three best parameters of each ultrasonic condition were selected for orthogonal optimization; the encapsulation efficiency (EE) of Qu and average particle size were used as evaluation indicators, and the comprehensive weighted scoring method was used to process the data of the evaluation indicators. The maximum EE and the minimum average particle size were set as 100 points, and the weight coefficient was set as 0.5. The comprehensive score was calculated according to the following formula:

$$\text{Comprehensive score} = 0.5 \times 100 \times (\text{EE}/\text{maximum EE} + \text{minimum average particle size}/\text{average particle size}) \quad (1)$$

The orthogonal test factor level table was shown in Table S1. The CPP-CS-Qu nanoparticles prepared under the optimal ultrasonic conditions (CPP-CS-Qu (US)) were divided into two parts, one part was immediately subjected to further analysis and application, and the other part was freeze-dried for subsequent analysis.

2.4. EE and loading capacities (LC)

The EE and LC of Qu were determined by a spectrophotometer as described by Liang, Ren, Zhang, Hou, Chalamaiah, Ma and Xu [14] with some modification. Briefly, freshly prepared colloidal dispersions were centrifuged at 10,000 g for 20 min to collect the undissolved Qu at 4 ℃. The obtained supernatant was then subjected to ultrafiltration using Millipore's Amicon Ultra-15 centrifugal filter devices with molecular weight cut-offs 10 kDa. The free Qu amount in the filtrate was measured using UV–Vis spectroscopy (Varian Inc., Palo Alto, USA) at $\lambda = 374$ nm. 1 to 12 μg/mL of Qu prepared and diluted with aqueous ethanol (80%, v/v) was used to establish a standard curve for the calculation of Qu content [20]. The EE and LC of Qu were calculated using the following equations:

$$\mathrm{EE}(\%) = (\text{Total Qu amount} - \text{Free Qu amount})/\text{Total Qu amount} \times 100\%$$

$$\mathrm{LC}(\%) = (\text{Total Qu amount} - \text{Free Qu amount})/\text{Total encapsulation amount} \times 100\% \quad (3)$$

2.5. Structural characterization

2.5.1. Intrinsic fluorescence spectrum

The fluorescence measurements were performed using a spectrofluorometer (Varian, Card F-98, USA). The concentration of fresh samples was adjusted to 0.25 mg/mL with HCl (pH 6.0). The experiment conditions were as follows: excitation and emission bandwidths, 10 nm and 5 nm; scanning speed, 100 nm/min; emission wavelength, 290–500 nm; excitation wavelength, 280 nm.

2.5.2. Fourier transform infrared (FTIR) spectroscopy

The lyophilized samples (1 mg) were mixed with KBr (11 mg) and pressed into slices with 1–2 mm. The FTIR of the samples were recorded by an infrared spectrophotometer (Thermo Nicolet Co., Nicolet iS50, USA) with scanning wavelengths from 4000 cm^{-1} to 400 cm^{-1}.

2.5.3. X-ray diffraction (XRD)

The crystalline structure was analyzed using a diffractometer (Bruker AXS, D8 Advance, German). The diffraction pattern of the samples from X-rays at 2θ was recorded ranging from 5° to 80° at a scanning rate of 5°/min. The instrument was operated at an acceleration voltage of 40 kV and a tube current of 40 mA.

2.5.4. Scanning electron microscopy (SEM)

The microstructures of the sample were observed by a scanning electron microscope (FEI Inc, Nova NanoSEM 450, USA). The freeze-dried sample was smeared onto an aluminum plate with a two-sided adhesive ztape and operated at an accelerating voltage of 5 kV.

2.5.5. Atomic force microscopy (AFM)

A drop of the sample (20 μL) was deposited on a mica matrix and placed in an incubator to evaporate the solvent at 25 °C. The AFM image was captured by a multimode atomic force microscope (Bruker Inc., Multimode8, Germany), which used a single crystal silicon cantilever needle to operate in ScanAsyst mode.

2.6. Determination of the stability

2.6.1. Effect of pH

The nanoparticle dispersions were adjusted to a range of pH values (3.0, 4.0, 5.0, 6.0 and 7.0) using 1 M HCl or 1 M NaOH. The particle size of samples was measured by the equipment of Malvern Nanosizer ZS (Malvern Inc., Malvern, UK). The experimental environment temperature is 25 ℃.

2.6.2. Effect of ionic strength

The NaCl solution was added to the nanoparticle dispersion so that the final NaCl concentration of the sample was 0, 25, 50, 100, 200 and 300 mM, respectively. The particle size of nanoparticle dispersions was measured as described in section 2.6.1.

2.6.3. Effect of exposure time

The freshly prepared free Qu and Qu-loaded nanoparticle dispersions were respectively filled into transparent glass bottles, and then placed in a light cabinet with 0.24 m^3) and exposed to ultraviolet (UV) light (wavelength 253.7 nm, power 20 W). Light stability was determined by measuring the retention rate of Qu after 0, 30, 60, 90, 120, 150, 180 and 210 min of ultraviolet light exposure [21]. The Qu in the sample was fully extracted with aqueous ethanol (80%, v/v), and its content was determined as described in section 2.4. The retention rate of Qu was calculated using the following equations:

$$\mathrm{Retentionrate}(\%) = \frac{\text{The determined Qu amount}}{\text{Total Qu amount}} \times 100\% \quad (4)$$

2.6.4. Effect of storage time

The freshly prepared Qu-loaded nanoparticle dispersions were stored at 4 °C in a dark and airtight condition for 28 d. The storage stability was determined by measuring the retention rate of Qu at a certain time interval (0, 2, 4, 7, 14, 28 d). The stored dispersion was centrifuged at 10,000 rpm for 5 min and the supernatant was subjected to determine the retention rate of Qu as described in section 2.6.3.

2.6.5. Simulated gastrointestinal digestion

Simulated gastrointestinal digestion was conducted according to the method as described by Chen et al. with slight modification [22]. After adjusted to pH 2.0 with 1 M HCl, 40 mL dispersion of fresh sample was preheated in a shaker (37 °C, 100 rpm) for 10 min; 26.7 mg of pepsin was added and mixed well to start simulating gastric digestion for 1 h. Then 13.6 mg of pancreatin, 200 mg of bile salts were added after adjusting the concentration of KH_2PO_4 to 0.05 M and pH to 7.4 with 5.0 M NaOH; this mixture was further incubated for 6 h in a shaking water bath (37 °C, 100 rpm). During the entire simulated digestion process, 3 mL of digested samples were collected at different simulated digestion times (0, 30, 60, 90, 120, 150, 180 min) for analysis.

2.7. Determination of antioxidant activity

2.7.1. DPPH· Radical scavenging activity

The DPPH radical scavenging activity of the sample was determined as described by Tatjana, Nikola, Aleksandar, Dubravka, JJelena, ZZorana and Boris [23] with slight modifications. The sample (2 mL) was

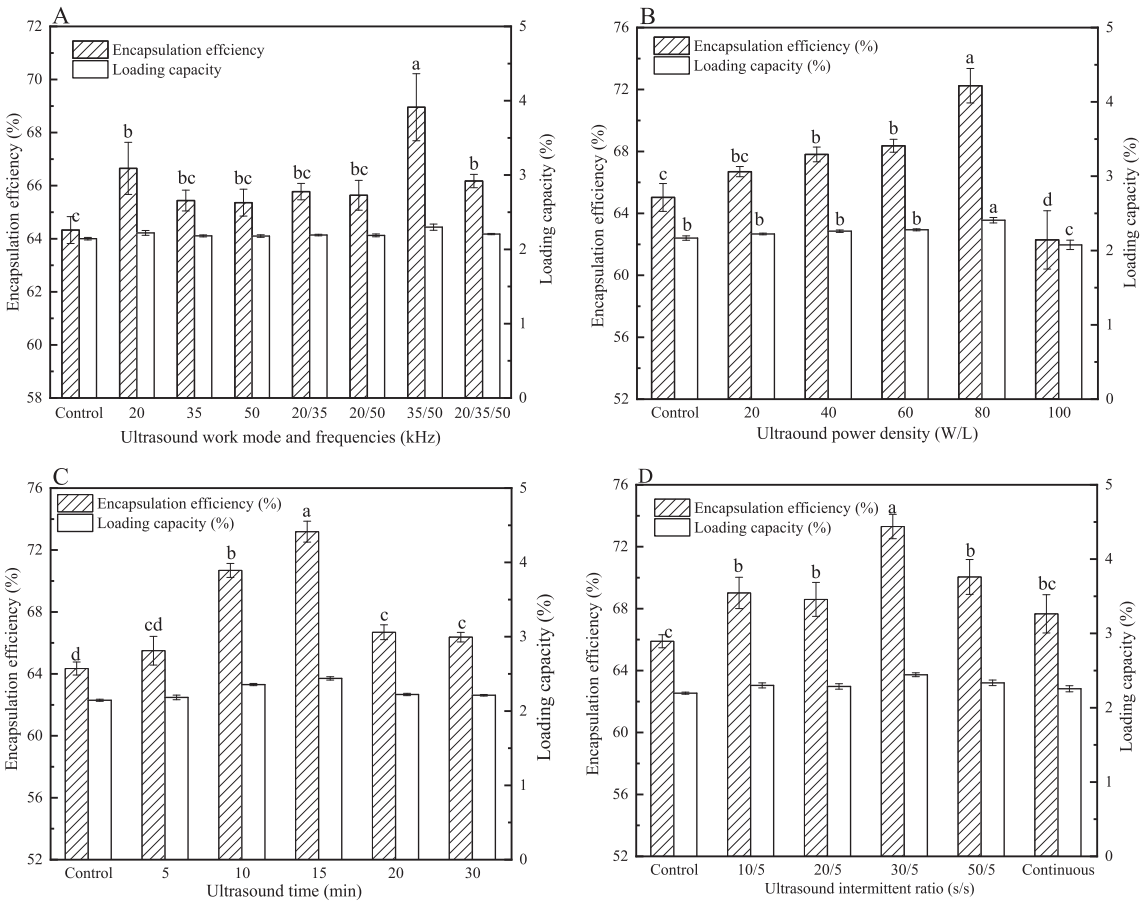

Fig. 1. Effects of ultrasound treatment with working mode and different frequency and (A), power density (B), time (C) and intermittent ratio (D) on the encapsulation efficiency and loading capacity of quercetin by casein phosphopeptides/chitosan complex coacervation. Different letters indicate significant differences ($p < 0.05$).

added to 2 mL of 0.2 mM DPPH (dissolved in absolute ethanol) and mixed thoroughly. After reacting for 30 min at 37 °C in the dark, the absorbance of the reaction solution was immediately read at 517 nm. The scavenging rate was calculated as follows:

DPPH· radical scavenging rate (%) = $[1\text{-}A_1/A_0] \times 100$ (5)

Where A_0 was the absorbance of the control, which was prepared using distilled water instead of the sample; A_1 was the absorbance of the sample.

2.7.2. ABTS· Radical scavenging activity

The ABTS· radical scavenging activity was determined according to the method described previously [24]. ABTS· radicals were produced by mixing ABTS (7.4 mM) and potassium persulfate (2.6 mM) at a ratio of 1:1 (v/v), and reacting for 16 h in the dark at 25 ℃. Then the ABTS solution was diluted with 10 mM PBS pH 7.0 until its absorbance value was 0.6–0.8 at 734 nm. 100 μL of the samples were added to 4 mL of diluted ABTS solutions and mixed thoroughly. The absorbance of the mixture was measured at 734 nm after reacting for 6 min at 37 °C. The ABTS· scavenging rate was calculated as follows:

ABTS· scavenging rate (%) = $[1\text{-}(A_1)/A_0] \times 100$ (6)

Where A_0 is the absorbance of the blank, $A1$ is the absorbance of the sample.

2.7.3. Reducing ability

The reducing power was measured according to the method of Oyaizu [25] with some modifications. 2.5 mL of the sample was mixed with 2.5 mL 1% potassium ferricyanide and then the mixture was incubated for 20 min at 50 ℃. After incubation, 2.5 mL of 10% TCA was added to terminate the reaction. Then 2 mL of supernatant of the above mixture was taken off and mixed with 2 mL of distilled water, and 0.5 mL of 0.01% ferric chloride. After standing at room temperature for 10 min, the absorbance of the resulting mixture was read at 700 nm; the greater the absorbance, the stronger the reduction ability.

2.8. Statistical analysis

All experiments were carried out in triplicate, and the result was expressed as mean ± standard deviation. Through the program SPSS Statistics 19.0 (SPSS Inc., Chicago, IL, USA), analysis of variance and Tukey's test were used for the data analysis, and a p value of < 0.05 was of significant difference. The corresponding graphs were drawn using the software OriginPro8.5 (Origin Lab Corporation, Northampton, MA, USA).

3. Results and discussion

3.1. Effect of ultrasonic treatment on the EE and LC of Qu by CPP/CS complex

Ultrasound can be categorized into several different regions along the frequency spectrum. Among them, power ultrasound (16–100 kHz) is characterized by a large bubble resonance size, followed by violent bubble collapse, which usually produces strong physical effects including local shear and high temperature. Therefore, power ultrasound is usually selected for emulsification, homogenization, cell disruption, polymerization and encapsulation [19]. The Qu-loaded CPP/CS nanoparticles were prepared by multi-frequency power ultrasound at different frequencies, power intensities, work time, and intermittent

ratio. EE and LC are the crucial parameters for evaluating the feasibility of ultrasound-assisted encapsulation delivery systems for potential applications. Fig. 1 shows the effects of ultrasound work conditions on the EE and LC of Qu. Results illustrated that ultrasound treatment could not affect the LC of Qu. In contrast, the EE of Qu increased obviously under ultrasound treatment. The above result indicated that there might be more macromolecular structures that could be stretched by ultrasound treatment, which interacted with more Qu, so that the EE could be improved. The fact that the LC remained unchanged might be attributed to an increase in the content of the CPP/CS complex utilized to load Qu. Compared to the control group (EE, 64.32%), all ultrasound work modes and frequencies can significantly ($p < 0.05$) improve the EE of Qu (Fig. 1A). The synchronous dual-frequency (35/50 kHz) ultrasound treatment had the best effect of all the ultrasound treatments, and its EE was maximized. This finding was consistent with our earlier work, which discovered that a certain combination of simultaneous dual-frequency ultrasonic processing might generate nanoparticles with higher EE [14]. The mutual interference or superposition of two frequencies (35 kHz and 50 kHz) might produce more resonance with the complex encapsulation system, which was conducive to the expansion of the macromolecular structure and the strengthening of the interaction between molecules, leading to an increase in the EE of Qu. The effects of ultrasonic power intensity on Qu's EE and LC can be seen in Fig. 1BThe EE and LC of Qu progressively rose as the power intensity increased, reaching the maximum (74.24%) at 80 W/L, which was 12.35% higher than that of the control (ultrasound untreated nanoparticles). The sonochemical yield will increase as the ultrasound power intensity is increased [26], which could help to improve the EE. Sutkar and Gogate [27] ascribed this phenomenon to the enhanced cavitation effect due to the slight increase in the collapse pressure, and the realization of more cavitation active volume and longer life. When the ultrasonic power was further increased to 100 W/L, the EE decreased significantly, indicating that excessive ultrasonic power might be not conducive to the formation of intermolecular non-covalent forces and the occurrence of embedding. As shown in Fig. 1C, ultrasound treatment time had a significant ($p < 0.05$) effect on the EE of Qu. The EE increased gradually as the operating time of the ultrasound treatment prolonged, reaching its maxima (73.43%) at 15 min and beyond that, the value was declined, even were lower than the control group. This result might be owing to differences in ultrasound times causing dynamic changes in the structures of CS and CPP, resulting in variations in exposed non-covalent bonds, changes in intermolecular interaction forces, and eventually a variety of EE of Qu by CPP/CS complex. Previous studies have also confirmed that controlling the ultrasound treatment time could result in macromolecular protein and polysaccharide with different structural properties, which were closely related to their functional properties [28]. Fig. 1D illustrated the effect of ultrasound intermittent ratio on the EE of Qu by the CPP/CS complex. Ultrasound intermittent ratio had a significant influence on the EE of Qu. It could be seen that the increase in the extent of EE of Qu obtained was higher in the case of ultrasound having the intermittent ratio of 30 s/5s as compared to that obtained under other ultrasound intermittent ratios. Long-term continuous ultrasonic treatment might cause a substantial increase in the system temperature, which was difficult to be reduced instantaneously by water bath cooling. Therefore, the continuous rise in temperature might cause Qu inactivation and weaken the effect of the ultrasonic treatment to improve the embedding of the nanoparticles on Qu. On the contrary, frequent stops during the ultrasonic treatment might cause frequent interruption of the energy received by the complex system, which might be not enough to break up agglomerates, reduce the size of macromolecules and help the exposure of non-covalent bonds, thus failing to achieve the best encapsulation effect.

Based on the above single factor experiment, the $L_9(3^4)$ orthogonal experiment was further used to optimize the combination of ultrasonic conditions that were used to prepare the CPP-CS-Qu nanoparticles. Particle size is the crucial parameter for the preparation of stable

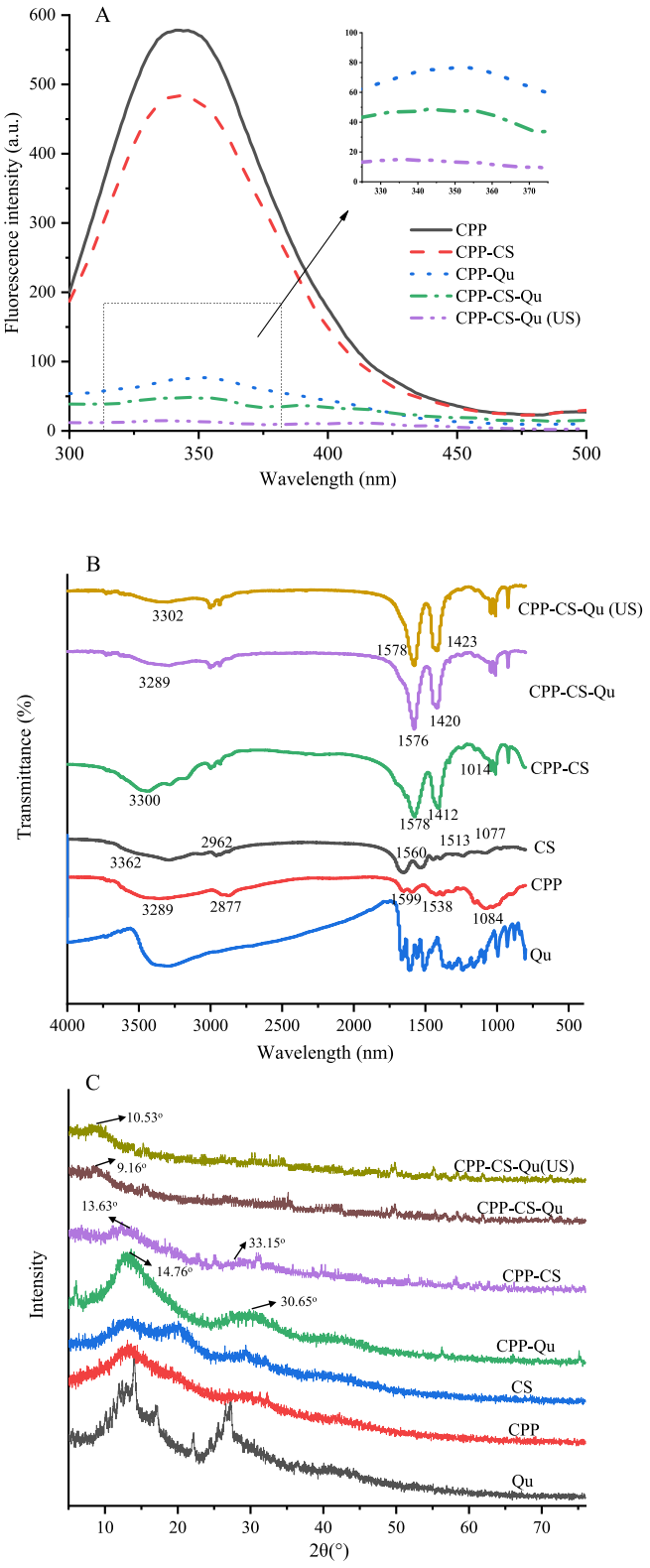

Fig. 2. Intrinsic fluorescence spectra (A), Fourier transform infrared spectra (B), and X-ray diffraction spectra (C) of the prepared samples. Qu, native quercetin; CPP, casein phosphopeptides; CS, chitosan; CPP-Qu, quercetin-loaded casein phosphopeptides nanoparticles; CPP-CS, quercetin-loaded chitosan nanoparticles; CPP-CS, casein phosphopeptides/chitosan complex coacervation; CPP-CS-Qu, quercetin-loaded casein phosphopeptides/chitosan nanoparticles; CPP-CS-Qu (US); quercetin-loaded casein phosphopeptides/chitosan nanoparticles prepared by ultrasound.

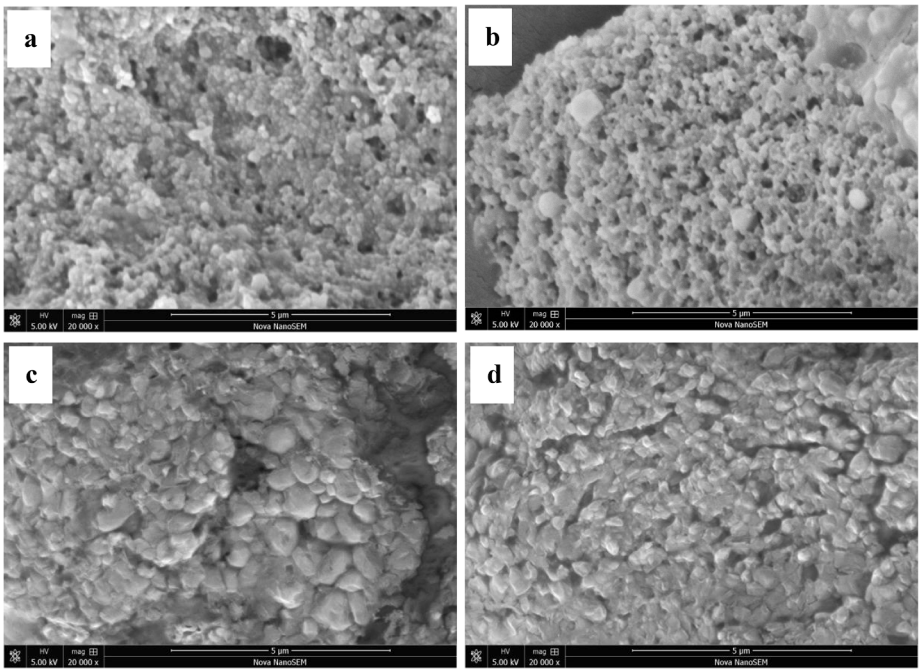

Fig. 3. Scanning electron microscopy images of the prepared samples. Qu, native quercetin; CPP-Qu, quercetin-loaded casein phosphopeptides nanoparticles; CPP-CS-Qu, quercetin-loaded casein phosphopeptides/chitosan nanoparticles; CPP-CS-Qu (US); quercetin-loaded casein phosphopeptides/chitosan nanoparticles prepared by ultrasound.

encapsulation for targeted nutrition and medical applications [29]. In addition to the EE of Qu, the average particle size was also included in the evaluation index. Results of the range analysis in Table S1 showed the influential orders of the four factors to weighted scorings were A > B > D > C; the optimal ultrasonic process conditions were $A_3B_2C_3D_1$, which implied that, the ultrasonic frequency, power, time and intermittent ratio were 20/35/50 kHz, 80 W/L, 20 min, and 20 s/5s, respectively. Additionally, Table S2 further validated the significant influence of the above four ultrasound factors on the encapsulation efficiency and average particle size of the CPP-CS-Qu nanoparticles. Since the optimal ultrasonic process conditions ($A_3B_2C_3D_1$) obtained from the above analysis were not present in the Table S1, the verification tests were performed and the resultswere: EE of Qu, 78.55 ± 0.70%; the average particle size, 241.27 ± 7.63 nm. As compared to the control group (EE, 64.32%; average particle size, 367.34 nm), the EE of the Qu of the CPP-CS-Qu nanoparticles prepared by ultrasound increased by 22.12%, and its average particle size was reduced by 34.32%. The CPP-CS-Qu nanoparticles prepared by the above optimal ultrasonic conditions were used for the following analysis of structure, environmental stability, and antioxidant activity.

3.2. Characterization of nanoparticles

3.2.1. Intrinsic fluorescence spectra

The fluorophore is sensitive to the polarity of the microenvironment of aromatic amino acid residues (tryptophan, tyrosine and phenylalanine); the interaction between proteins with the above amino acid residues and other molecules may cause fluorescence shift or fluorescence quenching [30]. Therefore, fluorescence is widely used to study molecular interactions between proteins and other substances. As presented in Fig. 2A, the emission fluorescence intensities of all samples (excited at wavelength of 280 nm) had a maximus value at about 340 nm, indicating that there was a large amount of tryptophan in CPPs. Obviously, the complex of CPP and CS decreased the fluorescence intensity of CPP. This was similar to the result of Hu, Wang, Li, Zeng and Huang [11] that CS could interact with peptides through hydrophobic interactions, resulting in a decrease in fluorescence intensity. While the fluorescence intensity of CPP-Qu and CPP-CS-Qu nanoparticles was much lower than that of CPP-CS nanoparticles; the combination of Qu and CPPs caused most fluorescence quenching of CPPs. Fluorescence quenching might be attributed to a variety of molecular interactions, including molecular rearrangement, ground-state complex formation, energy transfer, and collision quenching. [31]. In addition, compared with CPP, the λ_{max} of CPP-Qu and CPP-CS-Qu nanoparticles exhibited a red shift of about 9 nm, indicating that the combination of Qu and CPP might change the structure of CPP, stretch the polypeptide chain, and expose more hydrophobic group. It could be further speculated that there is a hydrophobic force between the molecules inside the nanoparticles. The fluorescence of CPP-CS-Qu (US) nanoparticles was reduced to almost zero, indicating that ultrasound enhanced the interaction between molecules including hydrophobic forces. However, after ultrasound treatment, there was no red shift appeared at the maximum wavelength. Similarly, Ma, Yan, Hou, Chen, Miao and Liu [32] prepared the soy protein isolate-citrus pectin complex and found that ultrasound treatment also reduced the fluorescence intensity of the SPI-CP complex without affecting λ_{max}. Jing et al. found that compared with the traditional alkaline/free radical method, the ultrasound-assisted method also did not change λ_{max} of egg white protein-tea polyphenol complexes [33].

3.2.2. FTIR spectra

FTIR was used to investigate the structural interaction of CPP-CS-Qu particles, as shown in Fig. 2B. The peaks of CPPs and CS were 3289 and 3362 cm^{-1}, respectively, indicating hydrogen bonding (3200–3400 cm^{-1}, N–H stretching) [34]. The complexation of CPPs and CS induced the formation of hydrogen bonds as the peaks shifted to 3439 cm^{-1}. The peak of CPP-CS-Qu nanoparticles at 3289 cm^{-1} is implied to the formation of a new hydrogen bond between the ternary complex resulted from its breakdown in the original binary complex. Interestingly, as compared to CPP-CS, the peak intensity of CPP-CS-Qu nanoparticles was greatly reduced. However, some studies have reported that encapsulating bioactive chemicals in protein/polysaccharides strengthens hydrogen bonds between molecules, resulting in a significant increase in peak intensity, which contradicts the findings of this study [35,36]. The FITR spectra of Qu revealed a large and broad peak in the opposite

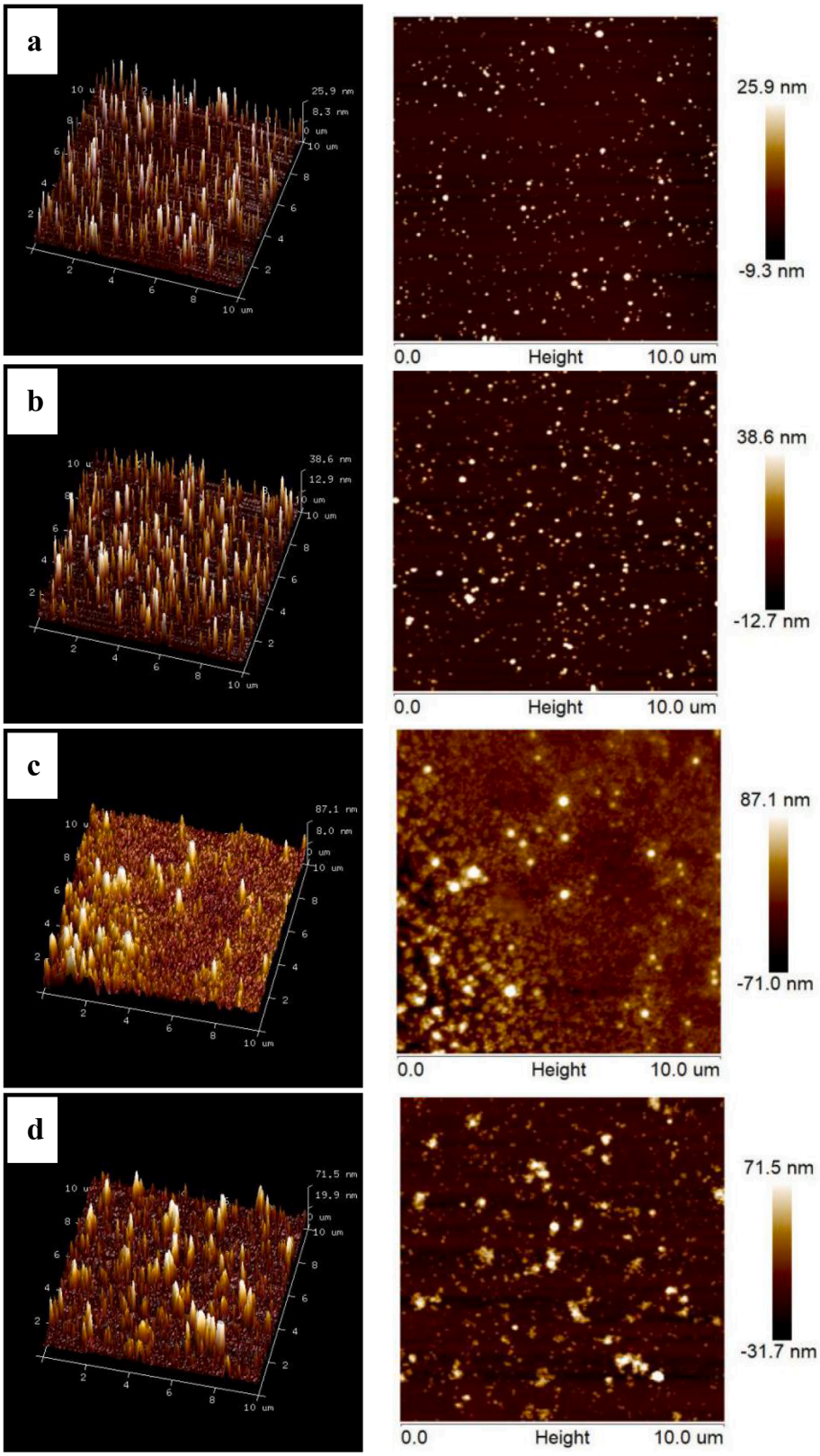

Fig. 4. Atomic force microscopy images of the prepared samples. Qu, native quercetin; CPP-Qu, quercetin-loaded casein phosphopeptides nanoparticles; CPP-CS-Qu, quercetin-loaded casein phosphopeptides/chitosan nanoparticles; CPP-CS-Qu (US); quercetin-loaded casein phosphopeptides/chitosan nanoparticles prepared by ultrasound.

direction near 3500 cm^{-1}. Therefore, it was inferred that the peak representing the hydrogen bond of the ternary complex might be masked by other peaks of Qu; a phenomenon appeared wherein the peak intensity representing the hydrogen bond was weakened. The CPPs also exposed characteristic peaks at 1655 cm^{-1} and 1538 cm^{-1}, representing the amide I band (1600–1700 cm^{-1}, C-O and C-N stretching) and the

amide II band (1400–1500 cm^{-1}, N–H deformation and C-N stretching), respectively [28]. It was found that the complexation of CPPs and CS shifted above peaks to 1578 cm^{-1} and 1412 cm^{-1} confirming the electrostatic interaction between protein and polysaccharide in addition to hydrogen bonds [15]. Hu, Wang, Li, Zeng and Huang [11] reported that ionic crosslinking of the $–NH3^{+}$ groups on CS to the $-PO4^{3-}$ groups on CPPs also played an important role in the complexation of CPPs and CS. Compared with the CPP-CS composite, the amide I and amide II bands of the CPP-CS-Qu nanoparticles moved to 1576 cm^{-1} and 1412 cm^{-1}, indicating that the encapsulation of Qu caused a change in electrostatic interaction. After ultrasound treatment, the hydrogen bond, amide I and II bonds remarkably red-shifted to 3302 cm^{-1}, 1578 cm^{-1} and 1423 cm^{-1} respectively. Furthermore, the peaks representing amide I and II bonds in CPP-CS-Qu were strengthened. This result showed ultrasound induced the stronger and more stable hydrogen bonding and electrostatic interactions among CPP, CS, and Qu, which was consistent with the results of intrinsic fluorescence spectra analyses. CPPs are a class of milk-derived bioactive peptides rich in phosphoserine (-Ser(P)-), with a core structure of -Ser (P)-Ser (P)-Ser (P)-Glu-Glu- [37]. The structure of CPPs was originally stretched, and there was no tertiary and quaternary structure. The CPPs themselves had more exposed groups than the macromolecular protein, and might be complexed with each other through non-covalent bonds. After ultrasound treatment, the interactions between the peptides themselves were broken. Moreover, the mechanical stirring effect of ultrasound might increase the contact and collision between polypeptides, polysaccharides, and Qu, thereby increasing their interactions.

3.2.3. XRD

The crystalline diffraction patterns of CS, CPP, Qu, CPP-Qu, CPP-CS,

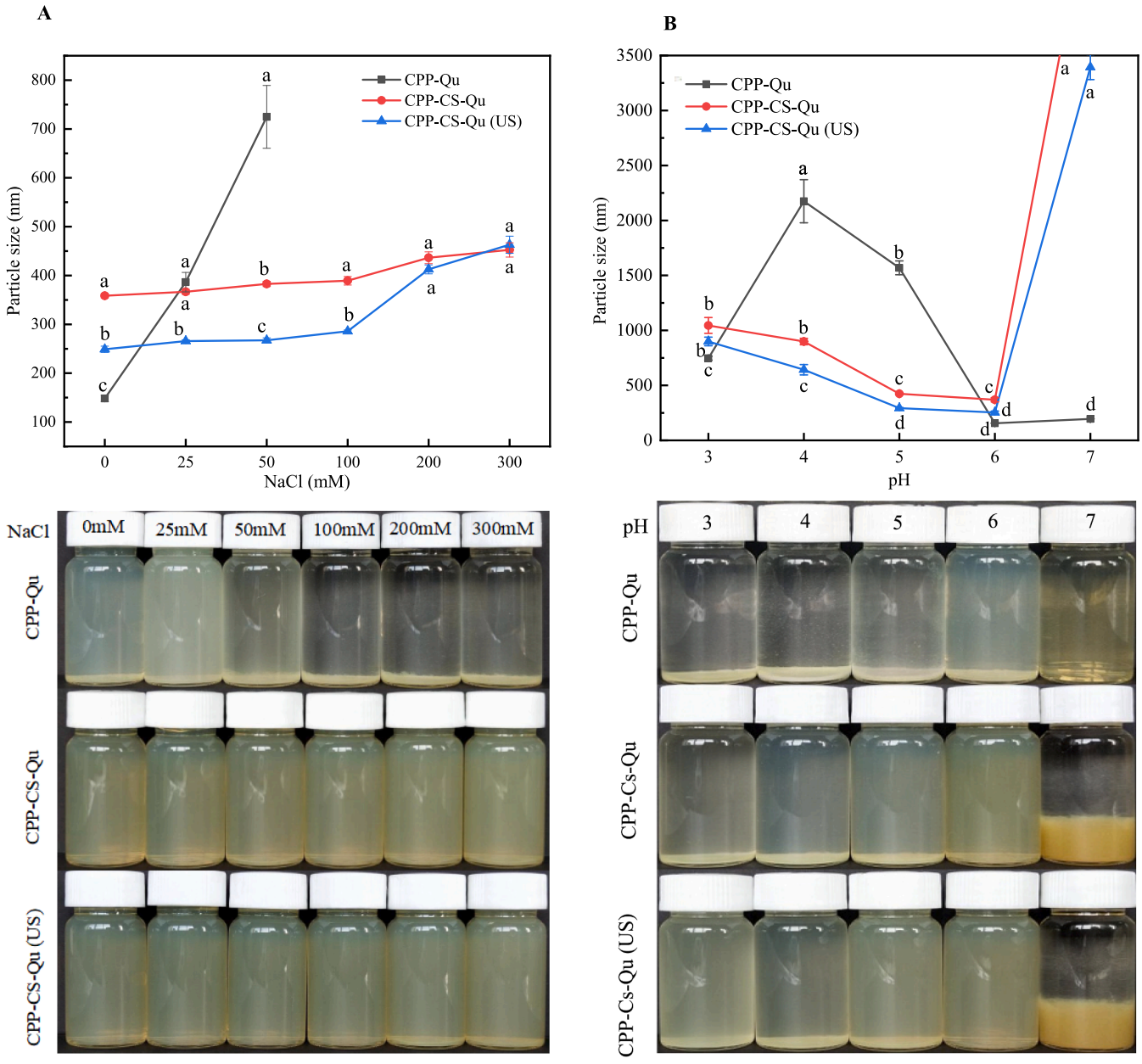

Fig. 5. Effect of pH (A) and NaCl concentration (B) on the particle size and visual appearance of the prepared samples. CPP-Qu, quercetin-loaded casein phosphopeptides nanoparticles; CPP-CS-Qu, quercetin-loaded casein phosphopeptides/chitosan nanoparticles; CPP-CS-Qu (US); quercetin-loaded casein phosphopeptides/chitosan nanoparticles prepared by ultrasound. Different letters indicate significant differences ($p < 0.05$).

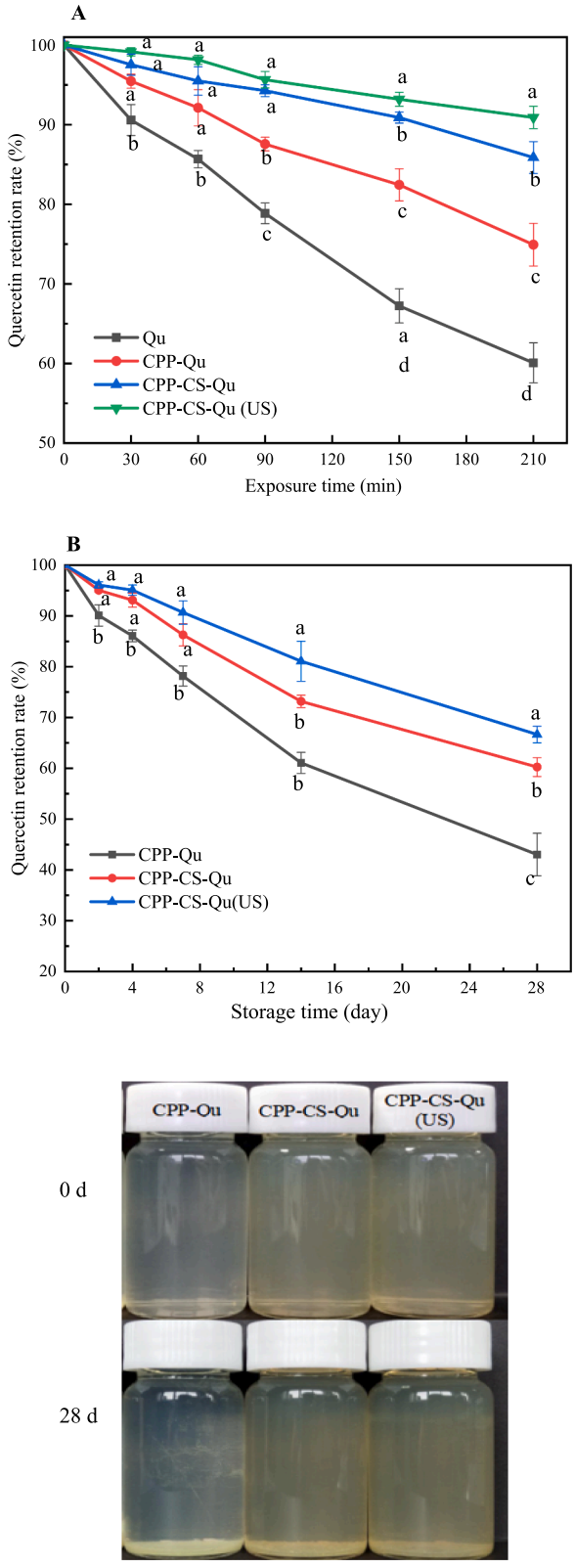

Fig. 6. Effect of ultraviolet radiation (A) and storage time (B) on the quercetin retention rate and visual appearance of the prepared samples. Qu, native quercetin; CPP-Qu, quercetin-loaded casein phosphopeptides nanoparticles; CPP-CS-Qu, quercetin-loaded casein phosphopeptides/chitosan nanoparticles; CPP-CS-Qu (US); quercetin-loaded casein phosphopeptides/chitosan nanoparticles prepared by ultrasound. Different letters indicate significant differences ($p < 0.05$).

CPP-CS-Qu, CPP-CS-Qu (US) are shown in Fig. 2C. There were some sharp peaks for pure Qu, reflecting its crystalline state [3]. In contrast, CPP and CS presented two flat peaks at diffraction angles 2θ of 16.01° and 32.24°, 16.34° and 20.08°, respectively, reflecting the amorphous nature of the polysaccharide and protein [38]. Except for the peaks at 14.76° and 30.65° in the CPP-Qu nanoparticles, most of the sharp crystal characteristic peaks derived from Qu disappeared, indicating that the encapsulation of Qu by CPP did not completely transform the state of Qu from the crystalline state to the amorphous state. While, the embedding of Qu in the CPP-CS complex disappeared all its characteristic peaks, providing convincing evidence of encapsulation. It could be clearly seen in Fig. 4C that CPP was tightly attached to the CPP-Qu surface, thus achieving a complete encapsulation of Qu, which was mutually confirmed with the XRD of CPP-CS-Qu. Noteworthily, two characteristic new small peaks appeared on the pattern of the CPP-CS complex, with diffraction angles of 13.63° and 33.15°. This result could further prove that an amorphous CPP-CS complex was formed through intermolecular interaction, which might greatly contribute to CPP-CS for Qu embedding. After ultrasound treatment, the typical peak shape of CPP-CS-Qu was more rounded. Also, the peak was shifted from 10.53° to 9.160° with the increase in the peak intensity. This result provided an additional evidence of the noncovalent interaction change among CPP, CS, and Qu, which has been well confirmed by the results of FTIR.

3.2.4. Morphology

Morphology of the CPP, CPP-Qu, CPP-Cs-Qu and CPP-Cs-Qu (US) nanoparticles were investigated by SEM (Fig. 3) and AFM (Fig. 4). CPP had fine, uniform spherical particles, as seen in Fig. 3a; when combined with two-dimensional AFM images (Fig. 4a), particle size was calculated to be<100 nm. This result was consistent with the finding of Hu, Wang, Li, Zeng and Huang [11], where they observed spherical CPP particles with smooth surfaces using transmission electron microscopy. Small molecules CPP might move close to each other and aggregate through intermolecular interactions, and then formed spherical particles through some secondary structures such as α-helix, β-sheet, β-turn, and random coil. After encapsulation of Qu, the CPP-Qu (Fig. 3b) exhibited obvious larger spherical nanoparticles; the absolute height values of CPP-Qu (51.3 nm) (Fig. 4b) were significantly larger than that of CPP particles (35.2 nm), indicating Qu was successfully encapsulated in CPP. Furthermore, it could be seen that the CPP-Qu nanoparticles were not uniform, the surface was rough, and the particles appeared connected. This phenomenon was attributed to the fact that the addition of Qu changed the morphology of CPP and the formation of CPP-Qu particles led to the stronger interaction force between the particles. Obviously, CPP-CS-Qu exhibited a surface microscopic morphology that was significantly different from that of the CPP-Qu. The results of SEM (Fig. 3c) and AFM (Fig. 4c) mutually confirmed each other and showed that the particle size and the height distribution of CPP-CS-Qu particles were remarkably increased; it seemed that highly hydrophilic CS packed some individual CPP-Qu particles together and tightly adhered to the surface of the nanoparticles, forming the so-called core–shell structure. Wang, Fu, Chen, Shi, Li, Zhang and Shen [39] also reported β-carotene could be well encapsulated in zein-carboxymethyl CS complex, and most of the formed nanoparticles were clumped and connected with each other. Additionally, the boundary between CPP-CS-Qu and CPP-CS-Qu particles was not clear and even connected into one piece; this agreed with the previous study that the excess CS molecules adsorbed on the surface of the CPP interact and form a so-called “hair layer” [11]. After ultrasound treatment, most of the large aggregate CPP-CS-Qu particles were broken, the size distribution of nanoparticles became much more uniform. The absolute height values of the ternary complex were sharply decreased from 158.1 nm to 103.2 nm. It was worth noting that the particles were still connected, although the size of the nanoparticles was reduced. The above result indicated that ultrasound caused a series of changes in the CPP-CS-Qu nanoparticles; ultrasound might strengthen and even create core–shell structures in composite biopolymer particles,

which was similar to the research result of Ma, Jiang, Chen, Wang, McClements, Liu, Liu and Ngai [40]. Ultrasound treatment broke the inherent interaction force (both in molecular interior and intermolecular) of CPP-CS-Qu nanoparticles, which might make the molecules relatively independent and form a better dispersion. Furthermore, ultrasound caused a change in the molecular structure, exposing additional functional groups; when the frequency of collisions between molecules increased, the molecules move closer to each other through non-covalent interactions, forming the particles shown in Fig. 3d and Fig. 4d.

3.3. Stability of nanoparticles

Colloidal nanoparticle delivery systems could experience a series of environmental conditions such as pH, ionic strength, exposure time, and storage time in commercial products. Therefore, it is necessary to evaluate the effects of various environmental stresses on the stability of the complex nanoparticles. The impact of pH (3–7) on the particle size and visual appearance of the prepared nanoparticles was studied. As shown in Fig. 5, the CPP-Qu particles were unstable; especially at the pH 4 and 5, the particle size exceeded 1500 nm; and the small white aggregates could be clearly seen in the corresponding apparent image. While, the CPP-CS-Qu particles were tentatively stable at pH 4–6, indicating the addition of CS effectively prevented the turbidity and eventually precipitation of CPP-Qu particles. CS was viscous and soluble in dilute acid; in dilute acid, the β-1,4-glycosidic bond of CS could be broken and CS would be hydrolyzed to oligomeric CS with cationic groups, which could tightly adhere on the surface of CPP-Qu by interaction with the PO_4^{3-} ionic gelation [11]. The electrostatic repulsion between the formed CPP-CS-Qu nanoparticles might be stronger than that of CPP-Qu, which overcame van der Waals and hydrophobic effects, thus presenting a visible and stable colloidal solution state. The phenomenon that CPP-CS-Qu particles had a sharp increase in particle size and precipitation at pH 7 could be explained as the pH might be close to the isoelectric point of CS [11]. As the pH value increased, the protonation of the CS surface decreased, and the repulsive effect between particles even disappeared; therefore, rapid agglomeration of particles was formed [41]. After ultrasound treatment, the particle size of CPP-CS-Qu was significantly reduced within the detected pH range; the appearance of CPP-CS-Qu in the glass bottle was more uniform and clearer. Ultrasound has been well proven to have the ability to control particle size and make them more uniform [41].

The influence of ionic strength (NaCl, 0–300 mM) and particle size and visual appearance of the prepared samples were shown in Fig. 5B. Apparently, the particle size of CPP-Qu increased greatly with the increase of NaCl concentration; when the NaCl concentration exceeded 100 mM, the particles aggregated to form a visible precipitate. This result might be attributed to the addition of a high concentration of NaCl that changed the interaction between CPP-Qu nanoparticles; enough counter ions (Na^+, Cl^-) neutralized the charge of the nanoparticles, generating electrostatic shielding and weakening the intermolecular electrostatic repulsion, which lead to the aggregation and precipitation of nanoparticles [31]. However, CPP-CS-Qu particles exhibited excellent stability within the range of ion concentration, even though the colloidal particles increased slightly from 248 nm to 436 nm with the increase of NaCl concentration. On the contrary, Dai, Li, Wei, Sun, Mao and Gao [31] reported curcumin-loaded zein-rhamnolipid complex nanoparticles were highly unstable and their aggregations were formed at higher NaCl concentrations (100–300 mM). The difference might be related to the physicochemical properties of the polysaccharides and proteins involved in the encapsulation. The excellent ion resistance of CPP-CS-Qu nanoparticles might be attributed to the strong steric hindrance of CS adsorbed on CPP-Qu by electrostatic attraction. The particle size of CPP-CS-Qu (US) was significantly smaller than that of CPP-CS-Qu at 0–100 mM NaCl, indicating ultrasound treatment decreased the particle size of CPP-CS-Qu at a low concentration of NaCl. While, the increase in NaCl concentration more than 100 mM had the dominant influence of ionic strength on the size of nanoparticles.

The effect of UV light time on the Quretention rate of the prepared nanoparticles were shown in Fig. 6. With the prolongation of exposure time, the free Qu was quickly decomposed. When the exposure time reached 210 min, the retention rate was<60%, demonstrating once again that natural Qu was easily degraded by light, and that this was due to the oxidation and decarboxylation of the carbon ring on its primary chain [42]. Compared with free Qu, the degradation rate of Qu in CPP-Qu and CPP-CS-Qu nanoparticles tended to be slower; when exposed to 210 min, the retention rates were 74.92% and 85.87%, respectively indicating that CPP and CS as Qu transport carriers could effectively protect Qu and retard its degradation under UV radiation. Meng, Wu, Xie, Cheng and Zhang [38] reported that some functional groups such as aromatic amino acid residues and double bonds of proteins/peptides could absorb ultraviolet light, thereby enhancing the protection of Qu. Furthermore, the close interaction between the molecules caused Qu to be wrapped by CPP and CS layer by layer, providing a strong physical barrier for Qu so that the active groups of Qu were protected from environmental stress. Similarly, Cuevas-Bernardino, Leyva-Gutierrez, Jaime Vernon-Carter, Lobato-Calleros, Roman-Guerrero and Davidov-Pardo [21] also found that the complex of pea protein and soybean gum could improve Qu's ability to resist photooxidation; the reason might be that the thick polysaccharide layer formed in the ternary complex provided a strong physical barrier for Qu, thereby effectively reducing photochemical degradation. Additionally, the retention rate of Qu in CPP-CS-Qu (US) nanoparticles was better than that of CPP-CS-Qu nanoparticles; especially with the increase of the exposure time, the ability of Qu in the CPP-CS-Qu (US) nanoparticles to resist photolysis became more obvious. This indicated ultrasound-assisted preparation of CPP-CS-Qu nanoparticles could improve the resistance of Qu in nanoparticles to UV decomposition. CPP-CS-Qu (US) has a narrow, homogeneous particle size distribution and a compact structure, allowing each Qu to be well protected, as shown in Fig. 4, which supported the above experimental results.

The effect of storage time on the Qu retention rate and visual appearance of the three prepared nanoparticles was shown in Fig. 6B. With the extension of the storage time, the retention rate of Qu in the solution gradually decreased, and some nanoparticles were precipitated, indicating that the stability of the nanoparticles was reduced. The retention rate of Qu occurred in decreasing order within 28 d, where CPP-CS-Qu (US) (66.66%) > CPP-CS-Qu (60.24%) > CPP-Qu (43.03%). Therefore, it could be inferred that the stability of CPP-CS-Qu (US) nanoparticles was better than that of CPP-CS-Qu, followed by CPP-Qu. In fact, Qu is insoluble in water, and can't be detected in a water system. The stability of CPP-Qu in the solution could be attributed to the existence of a certain electrostatic repulsion between CPP-Qu particles. The higher stability of CPP-CS-Qu particles compared to CPP-Qu particles highlighted that, in addition to electrostatic stability, the steric stabilization mechanism imparted to the system by the CS coating was important to avoid coalescence and precipitation of nanoparticles. The retention rate of Qu of CPP-CS-Qu (US) particles was 66.66% on the 28th day, which was 11% higher than CPP-CS-Qu. This result indicated that ultrasound treatment significantly improved the stability of CPP-CS-Qu nanoparticles in the solution. Ma, Jiang, Chen, Wang, McClements, Liu, Liu and Ngai [40] reported that ultrasonic treatment could promote the dispersion of reactants and improve the dispersibility of biopolymers in solution. Ultrasound has also been fully proven to effectively reduce the zeta potential and PDI of the ternary complex (zein-gum Arabic-resveratrol), which is beneficial to its stability in the solution medium. Furthermore, the efficient intense-shear forces generated during ultrasonic cavitation could be used to create small and relatively uniform nanoparticles [19]. On the other hand, ultrasound might break the original non-covalent force between the ternary complexes, cause certain changes in the structure of CPP and CS, exposing more functional groups, and establishing new and more stable intermolecular forces.

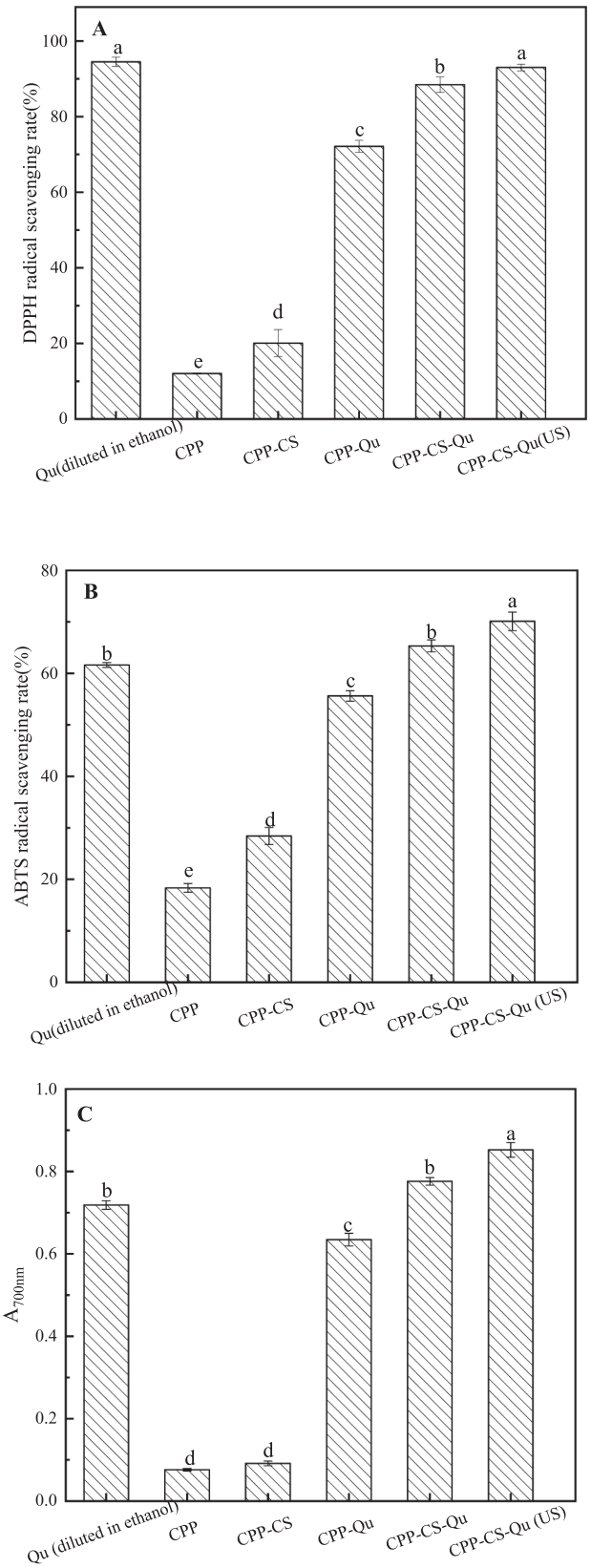

Fig. 7. DPPH· radical scavenging activity (A), ABTS· radical scavenging activity (B) and ferric reducing power (C) of the prepared samples. Qu, native quercetin diluted in ethanol; CPP, casein phosphopeptides; CPP-CS, quercetin-loaded chitosan nanoparticles; CPP-Qu, quercetin-loaded casein phosphopeptides nanoparticles; CPP-Qu, quercetin-loaded casein phosphopeptides nanoparticles; CPP-CS-Qu, quercetin-loaded casein phosphopeptides/chitosan nanoparticles; CPP-CS-Qu (US); quercetin-loaded casein phosphopeptides/chitosan nanoparticles prepared by ultrasound. Different letters indicate significant differences ($p < 0.05$).

Both these above reasons were beneficial to maintain the stability and longevity of the CPP-CS-Qu nanoparticles in the solution system.

3.4. Antioxidant activity

The DPPH radical scavenging activity, ABTS· radical scavenging activity and reducing ability were tested to evaluate the antioxidant capacity of Qu. As Qu is almost insoluble in water, and it is difficult to exhibit antioxidant activity in an aqueous solution; however, it has strong antioxidant activity in its ethanol-soluble state, such as its DPPH· and ABTS· radical scavenging rate of 94.52% and 61.63%, respectively, and a strong reduction ability with an absorbance of 0.7 (Fig. 7). The DPPH scavenging abilities of CPP-Qu, CS-Qu and CPP-CS-Qu were 72.14%, 88.47% and 95.5%7, respectively, indicating that CPP-CS-Qu nanoparticles exhibited stronger scavenging ability than CPP-Qu and CS-Qu nanoparticles. Meng, Wu, Xie, Cheng and Zhang [38] found a similar phenomenon that zein/carboxymethyl dextrin-curcumin nanoparticles showed higher DPPH· scavenging activity than carboxymethyl dextrin-curcumin and zein- curcumin nanoparticles. This result might also be related to the fact that the embedding of Qu in the CPP-CS complex allowed Qu to be evenly dispersed in the solution system, thereby increasing the full contact between Qu and the free radical, and helping Qu to exert its antioxidant activity. After ultrasound treatment, the DPPH· radical scavenging rate of CPP-CS-Qu was significantly improved and was comparable to that of free Qu diluted in ethanol. Ultrasonic treatment might change the interaction force between nanoparticle molecules, allowing the nanoparticles to reorganize and become more stable. [43]. The changes in the physicochemical properties of the nanoparticles caused by ultrasound might eventually make it easier for the conjugated diene structure of the embedded Qu to provide protons for DPPH, thereby improving the free radical scavenging ability of Qu. The analysis results of the other two antioxidant indexes (ABTS free radical scavenging activity and reducing ability) of the prepared nanoparticles were similar to the DPPH free radical scavenging activity. Furthermore, the ABTS· free radical scavenging activity and reducing ability of CPP-CS-Qu were almost equivalent to that of free Qu diluted in ethanol, and the above two indicators of CPP-CS-Qu (US) were even higher than that of free Qu diluted in ethanol. This result was attributed to the contribution of the antioxidant activity of CPP and CS

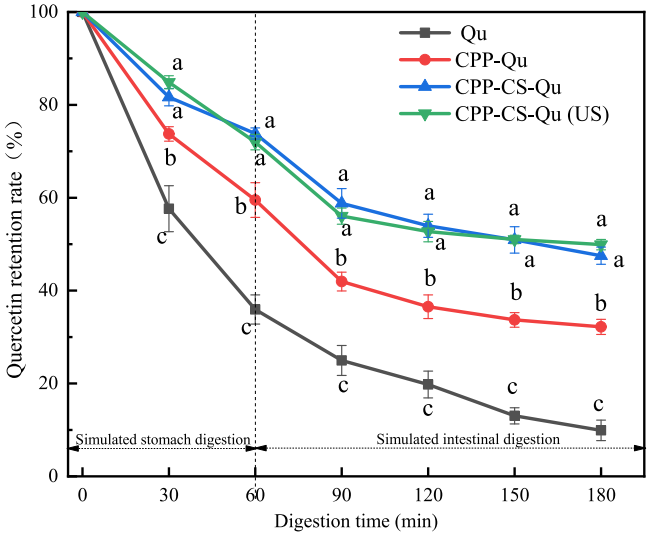

Fig. 8. Effect of simulated gastrointestinal digestion on the quercetin retention rate of the prepared samples. Qu, native quercetin; CPP-Qu, quercetin-loaded casein phosphopeptides nanoparticles; CPP-CS-Qu, quercetin-loaded casein phosphopeptides/chitosan nanoparticles; CPP-CS-Qu (US); quercetin-loaded casein phosphopeptides/chitosan nanoparticles prepared by ultrasound. Different letters indicate significant differences ($p < 0.05$).

in the CPP-CS-Qu nanoparticles [44]. The antioxidant activity of chitosan was related to the –OH group (C6) and –NH2 group (C2) of chitosan [45]; CPP has been widely reported to have antioxidant activity, which could directly scavenge free radicals and sequester potential metal pro-oxidants [46]. Additionally, Ultrasonic treatment optimized the antioxidant activity of the ternary complex by adjusting the interaction force and structure among molecules. In general, the above results suggested that the encapsulation of Qu in CPP/CS nanoparticles could help it exhibit antioxidant activity in an aqueous solution. Furthermore, the ultrasonic treatment proved an effective approach for increasing the antioxidant capacity of CPP-CS-Qu nanoparticles.

3.5. In vitro stability of Qu-loaded nanoparticles

The retention rates of free Qu, CPP-Qu, CPP-CS-Qu, and CPP-CS-Qu (US) nanoparticles were investigated to reflect their stability in simulated gastrointestinal digestion. As shown in Fig. 8, the retention rate of free Qu gradually decreased; when digested for 180 min, the retention rate was about 10%, indicating that Qu had almost lost its biological activity after digestion. Ma, Huang, Yin, Yu and Yang [47] also reported that the bioaccessibility of free quercetin in corn oil was 9.69% after *in vitro* digestion. Encapsulation of Qu could significantly increase the retention rate of Qu in the gastrointestinal tract, although part of Qu was still degraded, indicating that the encapsulation achieved a controlled release effect. This might be related to the existence of hydrogen bonds and strong hydrophobic interactions between Qu and the delivery vehicle. The retention rate of Qu in CPP-Qu nanoparticles was lower than that in CPP-CS-Qu nanoparticles. This could be explained by the fact that the hydrophilic shell of CS might prevent enzymatic degradation of the CPP in the gastrointestinal environment. CS has been well reported to resist the digestion of pepsin and pancreatin to a certain extent. The CPP-CS complex provided better protection of encapsulated Qu. Ultrasound treatment has no significant effect on the retention rate of Qu in the ternary nanoparticles. Additionally, it was noteworthy that after 30 min of simulated intestinal digestion, the retention rate of Qu in CPP-CS-Qu and CPP-CS-Qu (US) nanoparticles was 47.51% and 49.01% respectively, which tended to be stable, indicating this part of Qu stably existed in the intestine in the form of nanoparticles. Because of its mucoadhesive characteristics, CS can promote the penetration of bioactive substances, and this ability has generated considerable interest as a potential enhancer of transmucosal epithelial absorption[48]. It could be speculated that the CPP-CS-Qu and CPP-CS-Qu nanoparticles might be directly absorbed by the upper wall of the small intestine, thus giving full play to the physiological activity of Qu. It can also be concluded that embedding Qu in the CPP-CS complex will help increase Qu's bioavailability.

4. Conclusions

In the present study, CPP-CS complex was successfully prepared to encapsulate Qu by multi-frequency power ultrasound. The best ultrasonic conditions were optimized by single factor test and orthogonal experiments, and were ultrasonic frequency, 20/35/50 kHz; the power density, 80 W/L; the time, 20 min, and the intermittent ratio, 20 s/5s. Ultrasound had a significant effect on Qu's EE, while it had the opposite result for LC of Qu. After ultrasound treatment, the intermolecular interactions (hydrogen bonds, electrostatic interactions, and hydrophobic effects) among CPP, CS, and Qu were largely changed and further strengthened, which were demonstrated via fluorescence spectrum, XRD, and FTIR analysis. SEM and AFM images showed that the ternary composite nanoparticles undergoing ultrasonic treatment had a smooth surface, and their particle size was smaller and more uniform. Ultrasound further enhanced the antioxidant activity, acid, photochemical, salt, and storage stability of CPP-CS-Qu nanoparticles, although the above indicators were significantly improved by the addition of CPP. Furthermore, the composite nanoparticles prepared by ultrasound

treatment still exhibited excellent stability in simulated gastrointestinal digestion. Thus, this work proves the significance of ultrasound treatment to improve the recombination between CPP and CS, thereby modulating the encapsulation effect of Qu, the environmental stability and antioxidant activity of the formed ternary complex nanoparticles. The present study indicated that CPP-CS complex prepared by ultrasound has great potential for delivery of Qu and can be used in the pharmaceutical and food industry. However, further cell experiments and *in vivo* experiments are needed for better understanding of the bioavailability of Qu in the ternary nanoparticles prepared by ultrasound.

CRediT authorship contribution statement

Qiufang Liang: Investigation, Writing – original draft, Writing – review & editing, Funding acquisition. **Xinru Sun:** Data curation, Investigation, Methodology, Formal analysis. **Husnain Raza:** Software, Validation, Writing – review & editing. **Muhammad Aslam Khan:** Writing – review & editing. **Haile Ma:** Supervision, Writing – review & editing. **Xiaofeng Ren:** Conceptualization, Funding acquisition, Project administration, Resources, Supervision.

Declaration of Competing Interest

The authors declare that they have no known competing financial interests or personal relationships that could have appeared to influence the work reported in this paper.

Acknowledgements

The authors will express their appreciation for the support from the funds as follows: National Natural Science Foundation of China (funding number: 32072355 & 31771977); The Jiangsu agricultural science and technology innovation fund (Grants No. CX (20) 3044); The Primary Research & Development Plan of Zhenjiang (Grants No. NY2020011); Qinglan Project Funding (2020); Jiangsu Provincial Postdoctoral Science Foundation Special Funding Project (2019K114); Jiangnan University State Key Laboratory of Food Science and Technology Open Project (No.SKLF-KF-201701); Jiangsu University Young Key Teacher Program; Jiangsu Provincial Higher Education Key Discipline Development Project (PAPD)). There is no conflict of interest to declare. This article does not contain any research involving human or animal subjects.

Appendix A. Supplementary data

Supplementary data to this article can be found online at https://doi.org/10.1016/j.ultsonch.2021.105830.

References

[1] G. D'Andrea, Quercetin: A flavonol with multifaceted therapeutic applications? Fitoterapia 106 (2015) 256–271.
[2] G.E. Batiha, A.M. Beshbishy, M. Ikram, Z.S. Mulla, M.E. Abd El-Hack, A.E. Taha, A. M. Algammal, Y.H.A. Elewa, The Pharmacological Activity, Biochemical Properties, and Pharmacokinetics of the Major Natural Polyphenolic Flavonoid: Quercetin, Foods 9 (2020) 16.
[3] H. Li, D. Wang, C. Liu, J. Zhu, M. Fan, X. Sun, T. Wang, Y. Xu, Y. Cao, Fabrication of stable zein nanoparticles coated with soluble soybean polysaccharide for encapsulation of quercetin, Food Hydrocolloids 87 (2019) 342–351.
[4] Z. Chavoshpour-Natanzi, M. Sahihi, Encapsulation of quercetin-loaded β-lactoglobulin for drug delivery using modified anti-solvent method, Food Hydrocolloids 96 (2019) 493–502.
[5] P. Kumar, V. Pillay, G. Modi, Y.E. Choonara, C. Lisa, D. Naidoo, Self-Assembling Peptides: Implications for Patenting in Drug Delivery and Tissue Engineering, Recent Patents on Drug Delivery & Formulation 5 (2011) -.
[6] Y. Jiao, X. Zheng, Y. Chang, D. Li, X. Sun, X. Liu, Zein-derived peptides as nanocarriers to increase the water solubility and stability of lutein, Food & Funct. 9 (2018) 117.
[7] M. Lan, Y.u. Fu, H. Dai, L. Ma, Y. Yu, H. Zhu, H. Wang, Y. Zhang, Encapsulation of β-carotene by self-assembly of rapeseed meal-derived peptides: Factor optimization and structural characterization, LWT- Food Sci. Technol. 138 (2021) 110456, https://doi.org/10.1016/j.lwt.2020.110456.
[8] Y. Tang, X. Zhang, J. Sun, J. Hu, F. Zhang, J. He, Peptide nanofilaments used for replica-molding: A combination of "bottom-up" and "top-down", Surf. Rev. Lett. 14 (02) (2007) 301–307.
[9] Y. Zhang, M. Zhao, Z. Ning, S. Yu, N. Tang, F. Zhou, Development of a Sono-Assembled, Bifunctional Soy Peptide Nanoparticle for Cellular Delivery of Hydrophobic Active Cargoes, J. Agric. Food Chem. 66 (16) (2018) 4208–4218.
[10] W. Wang, Z. Yang, S. Patanavanich, B. Xu, Y. Chau, Controlling self-assembly within nanospace for peptide nanoparticle fabrication, Soft Matter 4 (8) (2008) 1617, https://doi.org/10.1039/b801890a.
[11] B. Hu, S.S. Wang, J. Li, X.X. Zeng, Q.R. Huang, Assembly of bioactive peptide-chitosan nanocomplexes, J. Phys. Chem. B 115 (23) (2011) 7515–7523.
[12] B. Zhu, T. Hou, H. He, Calcium-binding casein phosphopeptides-loaded chitosan oligosaccharides core-shell microparticles for controlled calcium delivery: Fabrication, characterization, and in vivo release studies, Int. J. Biol. Macromol. 154 (2020) 1347–1355.
[13] C. Arzeni, K. Martínez, P. Zema, A. Arias, O.E. Pérez, A.M.R. Pilosof, Comparative study of high intensity ultrasound effects on food proteins functionality, J Food Eng. 108 (3) (2012) 463–472.
[14] Q. Liang, X. Ren, X.i. Zhang, T. Hou, M. Chalamaiah, H. Ma, B. Xu, Effect of ultrasound on the preparation of resveratrol-loaded zein particles, J. Food Eng. 221 (2018) 88–94.
[15] X. Ren, T. Hou, Q. Liang, X.i. Zhang, D.i. Hu, B. Xu, X. Chen, M. Chalamaiah, H. Ma, Effects of frequency ultrasound on the properties of zein-chitosan complex coacervation for resveratrol encapsulation, Food Chem. 279 (2019) 223–230.
[16] T. Koupantsis, E. Pavlidou, A. Paraskevopoulou, Flavour encapsulation in milk proteins – CMC coacervate-type complexes, Food Hydrocolloids 37 (2014) 134–142.
[17] O.A. Higuera-Barraza, C.L. Del Toro-Sanchez, S. Ruiz-Cruz, E. Márquez-Ríos, Effects of high-energy ultrasound on the functional properties of proteins, Ultrason. Sonochem. 31 (2016) 558–562.
[18] R. Cui, F. Zhu, Ultrasound modified polysaccharides: A review of structure, physicochemical properties, biological activities and food applications, Trends Food Sci. Technol. 107 (2021) 491–508.
[19] T.S.H. Leong, G.J.O. Martin, M. Ashokkumar, Ultrasonic encapsulation - A review, Ultrason. Sonochem. 35 (2017) 605–614.
[20] H. Chen, Y. Yao, Phytoglycogen improves the water solubility and Caco-2 monolayer permeation of quercetin, Food Chem. 221 (2017) 248–257.
[21] J.C. Cuevas-Bernardino, F.M.A. Leyva-Gutierrez, E.J. Vernon-Carter, C. Lobato-Calleros, A. Román-Guerrero, G. Davidov-Pardo, Formation of biopolymer complexes composed of pea protein and mesquite gum – Impact of quercetin addition on their physical and chemical stability, Food Hydrocolloids 77 (2018) 736–745.
[22] F.-P. Chen, S.-Y. Ou, C.-H. Tang, Core-Shell Soy Protein-Soy Polysaccharide Complex (Nano)particles as Carriers for Improved Stability and Sustained Release of Curcumin, J. Agric. Food Chem. 64 (24) (2016) 5053–5059.
[23] J. Tatjana, M. Nikola, P. Aleksandar, M. Dubravka, D. JJelena, T. ZZorana, M. P. Boris, The evaluation of phenolic content, in vitro antioxidant and antibacterial activity of Mentha piperita extracts obtained by natural deep eutectic solvents, Food Chem. 362 (2021), 130226.
[24] Z. Fang, X. Cai, J. Wu, L. Zhang, Y. Fang, S. Wang, Effect of simultaneous treatment combining ultrasonication and pH-shifting on SPI in the formation of nanoparticles and encapsulating resveratrol, Food Hydrocolloids 111 (2021), 106250.
[25] M. Oyaizu, Studies on Products of Browning Reaction Antioxidative Activities of Products of Browning Reaction Prepared from Glucosamine, The Japanese, Journal of Nutrition and Dietetics 44 (6) (1986) 307–315.
[26] Leong, Thomas, Ashokkumar, Muthupandian, Kentish, Sandra, THE FUNDAMENTALS OF POWER ULTRASOUND - A REVIEW, Acoust. Aust. (2011).
[27] V.S. Sutkar, P.R. Gogate, Design aspects of sonochemical reactors: Techniques for understanding cavitational activity distribution and effect of operating parameters, Chem. Eng. J. 115 (2009) 26–36.
[28] Q. Liang, X. Ren, W. Qu, X. Zhang, H. Ma, The impact of ultrasound duration on the structure of β-lactoglobulin, J. Food Eng. 292 (2021), 110365.
[29] S.R. Falsafi, H. Rostamabadi, E. Assadpour, S.M. Jafari, Morphology and microstructural analysis of bioactive-loaded micro/nanocarriers via microscopy techniques; CLSM/SEM/TEM/AFM, Adv. Colloid Interface Sci. 280 (2020), 102166.
[30] Y. Wei, C. Li, L. Zhang, L. Dai, S. Yang, J. Liu, L. Mao, F. Yuan, Y. Gao, Influence of calcium ions on the stability, microstructure and in vitro digestion fate of zein-propylene glycol alginate-tea saponin ternary complex particles for the delivery of resveratrol, Food Hydrocolloids 106 (2020), 105886.
[31] L. Dai, R. Li, Y. Wei, C. Sun, L. Mao, Y. Gao, Fabrication of zein and rhamnolipid complex nanoparticles to enhance the stability and in vitro release of curcumin, Food Hydrocolloids 77 (2018) 617–628.
[32] X. Ma, T. Yan, F. Hou, W. Chen, S. Miao, D. Liu, Formation of soy protein isolate (SPI)-citrus pectin (CP) electrostatic complexes under a high-intensity ultrasonic field: Linking the enhanced emulsifying properties to physicochemical and structural properties, Ultrason. Sonochem. 59 (2019), 104748.
[33] H. Jing, J. Sun, Y. Mu, M. Obadi, D.J. McClements, B. Xu, Sonochemical effects on the structure and antioxidant activity of egg white protein–tea polyphenol conjugates, Food & Funct. 11 (8) (2020) 7084–7094.

[34] Q. Liang, X. Ren, X. Zhang, T. Hou, M. Chalamaiah, H. Ma, B. Xu, Xu, Effect of ultrasound on the preparation of resveratrol-loaded zein particles, J. Food Eng. 221 (2018) 88–94.
[35] Y. Luo, Z. Teng, Q. Wang, Development of zein nanoparticles coated with carboxymethyl chitosan for encapsulation and controlled release of vitamin D3, J. Agric. Food Chem. 60 (3) (2012) 836–843.
[36] Y. Luo, B. Zhang, M. Whent, L.L. Yu, Q. Wang, Preparation and characterization of zein/chitosan complex for encapsulation of alpha-tocopherol, and its in vitro controlled release study, Colloids Surf. B Biointerfaces 85 (2011) 145–152.
[37] R. Hartmann, H. Meisel, Food-derived peptides with biological activity: from research to food applications, Curr. Opin. Biotechnol. 18 (2) (2007) 163–169.
[38] R. Meng, Z. Wu, Q.T. Xie, J.S. Cheng, B. Zhang, Preparation and characterization of zein/carboxymethyl dextrin nanoparticles to encapsulate curcumin: Physicochemical stability, antioxidant activity and controlled release properties, Food Chem. 340 (2021), 127893.
[39] M. Wang, Y. Fu, G. Chen, Y. Shi, X. Li, H. Zhang, Y. Shen, Fabrication and characterization of carboxymethyl chitosan and tea polyphenols coating on zein nanoparticles to encapsulate β-carotene by anti-solvent precipitation method, Food Hydrocolloids 77 (2018) 577–587.
[40] C. Ma, W. Jiang, G. Chen, Q. Wang, D.J. McClements, X. Liu, F. Liu, T. Ngai, Sonochemical effects on formation and emulsifying properties of zein-gum Arabic complexes, Food Hydrocolloids 114 (2021), 106557.
[41] Y. Gokce, B. Cengiz, N. Yildiz, A. Calimli, Z. Aktas, Ultrasonication of chitosan nanoparticle suspension: Influence on particle size, Colloids. Surface. A 462 (2014) 75–81.
[42] Y. Wang, X. Wang, Binding, stability, and antioxidant activity of quercetin with soy protein isolate particles, Food Chem. 188 (2015) 24–29.
[43] R. Cimino, S.K. Bhangu, A. Baral, M. Ashokkumar, F. Cavalieri, Ultrasound-Assisted Microencapsulation of Soybean Oil and Vitamin D Using Bare Glycogen Nanoparticles, Molecules 26 (2021) 12.
[44] B. Hu, Y. Ting, X. Zeng, Q. Huang, Bioactive peptides/chitosan nanoparticles enhance cellular antioxidant activity of (-)-epigallocatechin-3-gallate, J. Agric. Food Chem. 61 (4) (2013) 875–881.
[45] S. Roy, J.W. Rhim, Fabrication of chitosan-based functional nanocomposite films: Effect of quercetin-loaded chitosan nanoparticles, Food Hydrocolloids 121 (2021) 11.
[46] D.D. Kitts, Antioxidant properties of casein-phosphopeptides, Trends Food Sci. Tech. 16 (12) (2005) 549–554.
[47] J.J. Ma, X.N. Huang, S.W. Yin, Y.G. Yu, X.Q. Yang, Bioavailability of quercetin in zein-based colloidal particles-stabilized Pickering emulsions investigated by the in vitro digestion coupled with Caco-2 cell monolayer model, Food Chem. 360 (2021) 9.
[48] J.-F. Zhou, G.-D. Zheng, W.-J. Wang, Z.-P. Yin, J.-G. Chen, J.-E. Li, Q.-F. Zhang, Physicochemical properties and bioavailability comparison of two quercetin loading zein nanoparticles with outer shell of caseinate and chitosan, Food Hydrocolloids 120 (2021) 106959, https://doi.org/10.1016/j.foodhyd.2021.106959.